Ocean Surface Flux Algorithm Effects on Tropical Indo-Pacific Intraseasonal Precipitation

Chia-Wei Hsu[1], Charlotte A. DeMott[1], Mark Branson[1], Jack Reeves Eyre[2], and Xubin Zeng[3]

[1]Colorado State University
[2]University of Washington
[3]The University of Arizona

November 22, 2022

Abstract

Surface latent heat fluxes help maintain tropical intraseasonal precipitation. We develop a latent heat flux diagnostic that depicts how latent heat fluxes vary with the near-surface specific humidity vertical gradient (dq) and surface wind speed (|V|). Compared to fluxes estimated from |V| and dq measured at tropical moorings and the COARE3.0 algorithm, tropical latent heat fluxes in the NCAR CEMS2 and DOE E3SMv1 models are significantly overestimated at |V| and dq extrema. Madden–Julian oscillation (MJO) sensitivity to surface flux algorithm is tested with offline and inline flux corrections. The offline correction adjusts model output fluxes toward mooring-estimated fluxes; the inline correction replaces the original bulk flux algorithm with the COARE3.0 algorithm in atmosphere-only simulations of each model. Both corrections reduce the latent heat flux feedback to intraseasonal precipitation, in better agreement with observations, suggesting that model-simulated fluxes are overly supportive for maintaining MJO convection.

Ocean Surface Flux Algorithm Effects on Tropical Indo-Pacific Intraseasonal Precipitation

Chia-Wei Hsu [1], Charlotte A. DeMott, Mark D. Branson[1], Jack Reeves Eyre[2], and Xubin Zeng[3]

[1]Colorado State University, Fort Collins, CO, USA
[2]Cooperative Institute for Climate, Ocean and Ecosystem Studies, University of Washington, Seattle, WA, USA
[3]University of Arizona, Tucson, AZ, USA

Key Points:

- Latent heat flux shows significant differences between bulk flux schemes as a function of wind speed and humidity disequilibrium.
- Changing bulk flux schemes in model shows a more realistic latent heat flux contribution on maintaining precipitation.
- Latent heat flux difference due to bulk flux schemes are non-uniform during different MJO phases.

Corresponding author: Chia-Wei Hsu, Chia-Wei.Hsu@colostate.edu

Abstract

Surface latent heat fluxes help maintain tropical intraseasonal precipitation. We develop a latent heat flux diagnostic that depicts how latent heat fluxes vary with the near-surface specific humidity vertical gradient (Δq) and surface wind speed ($|\mathbf{V}|$). Compared to fluxes estimated from $|\mathbf{V}|$ and Δq measured at tropical moorings and the COARE3.0 algorithm, tropical latent heat fluxes in the NCAR CEMS2 and DOE E3SMv1 models are significantly overestimated at $|\mathbf{V}|$ and Δq extrema. Madden–Julian oscillation (MJO) sensitivity to surface flux algorithm is tested with offline and inline flux corrections. The offline correction adjusts model output fluxes toward mooring-estimated fluxes; the inline correction replaces the original bulk flux algorithm with the COARE3.0 algorithm in atmosphere-only simulations of each model. Both corrections reduce the latent heat flux feedback to intraseasonal precipitation, in better agreement with observations, suggesting that model-simulated fluxes are overly supportive for maintaining MJO convection.

Plain Language Summary

Surface latent heat flux from ocean to the atmosphere is one of the important processes that provides water vapor and energy to the daily tropical rainfall. In this study, a visually intuitive latent heat flux diagnostic is proposed to better understand the model shortfall on its latent heat flux representation. This diagnostic allows a simple assessment of model latent heat flux biases arising either from biases in water vapor or surface wind speed as well as other empirical coefficients in the model. We demonstrate that, compared to "observed" fluxes also estimated from water vapor and surface wind speed measured at tropical moorings, tropical latent heat fluxes in the NCAR CEMS2 and DOE E3SMv1 models are significantly overestimated when extreme water vapor or surface wind speed happens.

Both offline and inline latent heat flux correction is applied to simulated fluxes. For both models, the correction reduces the percentage of latent heat flux on supporting the rainfall over the tropics which is in better agreement with observations. Particularly, the latent heat flux correction are non-uniform across different stages of the Madden–Julian oscillation (MJO). This finding suggests that a model improvement on the latent heat flux representation will change the simulated MJO.

1 Introduction

Marine surface fluxes are the mechanism through which heat, momentum, water mass, and gases are transferred between the ocean and atmosphere. Surface sensible and latent heat fluxes play an important role in the tropical climate system by cooling the ocean surface, regulating the thermal properties of the marine boundary layer, and invigorating tropical convection through the release of latent heat when water vapor is recondensed in convective updrafts.

While equatorial latent heat fluxes are generally uncorrelated with precipitation over a wide range of scales, for some tropical disturbances, such as the Madden-Julian oscillation (MJO; Madden and Julian (1971, 1972)) and certain types of convectively-coupled equatorial waves (Kiladis et al., 2009), latent heat fluxes vary coherently with precipitation, and thus help maintain convection by replenishing column water vapor lost through precipitation formation (Dellaripa & Maloney, 2015; Yasunaga et al., 2019). Recent studies report that anomalous surface latent heat fluxes offset approximately 7–10% of column moisture lost to MJO precipitation formation (Araligidad & Maloney, 2008; Dellaripa & Maloney, 2015; DeMott et al., 2015, 2016; Bui et al., 2020). Small variations in the tropical surface latent heat flux-precipitation relationship may play an important role in regulating MJO periodicity and phase speed (Matsugishi et al., 2020), which may

then rectify onto the MJO teleconnection response that modulates the frequency of extreme weather events globally (Stan et al., 2017; Yadav & Straus, 2017).

In models, surface latent heat fluxes are parameterized using a variety of bulk flux algorithms that estimate the flux based on wind speed ($|\mathbf{V}|$), the vertical gradient of near-surface specific humidity (Δq), and an empirically-determined transfer coefficient. Brunke et al. (2003) demonstrated that many of the bulk flux algorithms used in modern climate models overestimate fluxes when compared to direct flux measurements from field campaigns, but the then-most recent version of the COARE algorithm (COARE3.0, hereafter referred to as COARE; (Fairall et al., 2003)) was one of the least problematic. Differences between COARE-estimated fluxes and those estimated from other widely used algorithms tend to be largest at low and high wind extremes (Zeng et al., 1998; Brodeau et al., 2017). Because winds throughout the MJO lifecycle vary from nearly calm to highly disturbed conditions (de Szoeke et al., 2015), fluxes estimated using different bulk flux formulae could alter the apparent surface flux feedback to the simulated MJO.

In this study, we introduce a surface flux diagnostic that illustrates how surface latent heat fluxes vary as a function of $|\mathbf{V}|$ and Δq, i.e. a "flux matrix". The diagnostic is applied to surface fluxes estimated with in situ data from tropical Pacific moorings and the COARE algorithm. It is then applied to output from two Earth system models. We use the observational result to estimate an "offline" surface flux correction and estimate the effect of the revised flux on MJO column moistening. This offline correction is then compared to MJO-flux feedbacks in model simulations where the native bulk flux algorithm is replaced with the COARE algorithm. Models and data are described in Section 2, and results of the flux matrix analysis are presented in Section 3. Offline and inline corrections to model surface fluxes are discussed in Sections 4 and 5, respectively, and conclusions are given in Section 6.

2 Models and observation

We analyze daily mean surface fluxes in two Earth system models, the NCAR Community Earth System Model, version 2 (CESM2; (Danabasoglu et al., 2020)) and the DOE Energy Exascale Earth System Model, version 1 (E3SMv1; (Golaz et al., 2019)). For offline surface flux assessments, we use CESM2 output (1998-2014) from the historical (ocean-atmosphere coupled) simulation produced for phase 6 of the Coupled Model Intercomparison Project (CMIP6; (Eyring et al., 2016)) (CESM2 hereafter) and E3SMv1 output from a historical (ocean-atmosphere coupled) simulation (1995-2014) with daily output (E3SMv1 hereafter). For the inline surface flux assessment, we use the E3SMv1 atmosphere-only simulation produced by Reeves Eyre et al. (2021) where the native bulk flux algorithm is replaced with the COARE bulk flux algorithm. In their experiment, the atmosphere only simulation is forced with repeating ocean and sea-ice data based on observation year of 2000 (E3SMv1_climo hereafter). For CESM2, we used the same code base developed by Reeves Eyre et al. (2021) for our inline experiments with a 1979-2009 AMIP-type (atmosphere-only) simulation (CESM2_amip hereafter).

Variables needed for our analysis include the daily mean latent heat flux (LH), rainfall (R), 10 meter wind speed ($|\mathbf{V}|$), 2 meter specific humidity (q_{2m}), surface temperature (T_{sfc}), and sea level pressure (P_{sfc}). We use sea surface temperature reduced by 0.2 K (Zeng et al., 1998; Donlon & the GHRSST-PP Science Team, 2005) to estimate the sea surface skin temperature if the simulation output does not provide surface temperature. T_{sfc} and P_{sfc} determine the saturated specific humidity (q^*_{sfc}) at the air-sea interface which is further used to calculate the disequilibrium of moisture at the surface ($\Delta q = 0.98q^*_{sfc} - q_{2m}$) where q^*_{sfc} is reduced by 0.02 to account for the reduction of q^* by salinity (Zeng et al., 1998). CESM2 in both CMIP6 and AMIP simulations provide all the listed variables. E3SMv1 CMIP6 simulation, on the other hand, provides $|\mathbf{V}|$

and q at 1000 hPa. We follow de Szoeke et al. (2012) to estimate T_{sfc} and q_{2m} (See supplemental information for additional details).

For observations, we use daily means of the above fields collected with the TAO/TRITON (McPhaden et al., 1998) and RAMA (McPhaden et al., 2010) mooring arrays over the tropical Pacific and the Indian Ocean. These data are available from the National Oceanic and Atmospheric Administration Pacific Marine Environmental Laboratory at `https://www.pmel.noaa.gov/gtmba/`. The latent heat flux measurement provided by the observation is based on the COARE3.5 bulk flux algorithm, which is the same as COARE 3.0 for latent heat flux (Edson et al., 2013). COARE is not a direct co-variance measurement of the surface flux, but provides one of the more accurate estimates of directly measured surface fluxes (Brunke et al., 2003; Brodeau et al., 2017).

For intraseasonal variability and the MJO, our region of interest is the tropical Indian Ocean and western tropical Pacific from November through April, when MJO events propagate farthest eastward (Zhang & Dong, 2004). For intraseasonal analysis, all time series are computed as anomalies from the mean annual cycle (i.e., the mean and first four harmonics) and then filtered using a 20-100 day band-pass Lanczos filter with 60 weights.

3 Latent heat flux matrix

The bulk form of the latent heat flux (LH) can be written as

$$LH = \rho L_v C_e |\mathbf{V}| \Delta q; \quad \Delta q = q^*_{sfc} - q_{2m} \tag{1}$$

where ρ is the near-surface air density, L_v is the latent heat of vaporization, C_e is the transfer coefficient, and $|\mathbf{V}|$ and Δq are the same as described above. Different algorithms use different parameterizations of C_e, which varies primarily as a function of $|\mathbf{V}|$, with additional sensitivity to stability of the marine boundary layer (Fairall et al., 2003), wind gustiness (Redelsperger et al., 2000) and ocean wave state (Bourassa et al., 1999).

Based on Eq. 1, we designed a latent heat flux matrix diagnostic. Using daily mean values over the tropical Indian Ocean and western tropical Pacific (20°S–20°N and 30°E–180°E), we average the latent heat flux values based on $|\mathbf{V}|$ with a 1 $m\ s^{-1}$ bin width, and Δq with a 1 $g\ kg^{-1}$ bin width (Figure 1a). We also calculate the frequency of occurrence for each $|\mathbf{V}|$–Δq bin. This diagnostic visually illustrates the relationship between LH, $|\mathbf{V}|$, and Δq, and allows for a more nuanced assessment of model latent heat flux biases than possible with seasonal mean difference maps.

The latent heat flux matrix from different datasets shows the discrepancies caused by the different transfer coefficients used in different bulk flux algorithms (Figure 1b-d). The latent heat flux biases from CESM2 and E3SMv1 are similar since they use the same bulk flux algorithm (Large & Yeager, 2004, 2009). The largest biases are found at extreme values of $|\mathbf{V}|$ and Δq, indicating that the models overestimate the flux in these conditions. Small differences in biases between CESM2 and E3SMv1 likely arise from uncertainties introduced when estimating E3SMv1 near-surface T, q, and $|\mathbf{V}|$ values from those reported at 1000 hPa (see Supplement). For the most frequently observed conditions (within the 1% white contours in Figure 1), latent heat flux biases range from -20 Wm^{-2} to 20 Wm^{-2} for both models, or 4-8% of the original latent heat flux values. These biases are statistically significant with 99% confidence.

4 Offline correction of latent heat flux and estimated effect on MJO

The offline correction to model latent heat fluxes is achieved by dividing all model fluxes within a given $|\mathbf{V}|$–Δq bin by the model-to-mooring flux ratio for that bin. Since it is an offline correction, the changes in the latent heat flux cannot affect the precip-

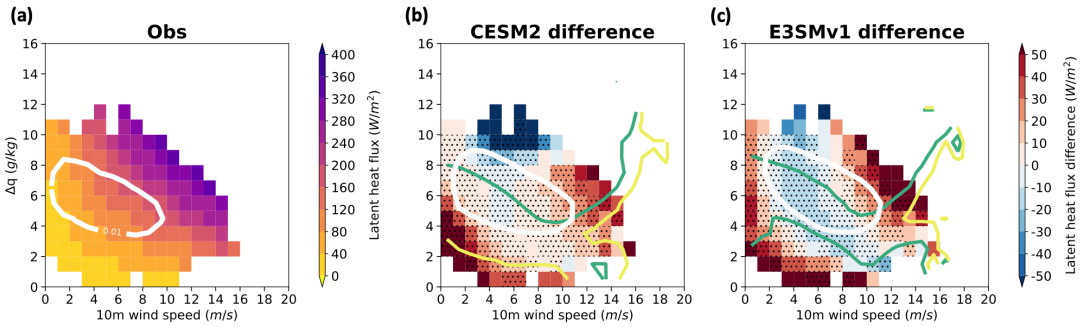

Figure 1. Latent heat flux (shading) binned by 10 m winds speed with 1 m/s width of each bin and the moisture disequilibrium (Δq) with 1 g/kg width based on (a) TAO/TRITON and RAMA array over the Indian Ocean and western tropical Pacific (Obs). The same binned latent heat flux matrix subtracts the Obs's latent heat flux matrix from (b) CESM2 and (c) E3SMv1. The dotted area means the biases are statistically significant with 99% confidence. The white thick contour line represents the probability of occurrence of 1%. The thin green and yellow contours represent the mean precipitation of 5 mm/day and 10 mm/day, respectively.

itation and circulations in the original simulation. This gives us a chance to quickly examine how large of a change in latent heat flux might be expected with the COARE algorightm given the $|\mathbf{V}|$ and Δq inputs of the existing simulation.

To understand how such changes to surface fluxes might affect the simulated MJO, we regress intraseasonal latent heat flux anomalies onto intraseasonal precipitation anomalies, where precipitation is expressed in units of W m^{-2} (Figure 2). As in Bui et al. (2020), we first focus on a small region in the western tropical Pacific (160°E-180° and 10°S-8°S). Based on satellite-derived observational data, Bui et al. (2020) showed that intraseasonal latent heat fluxes maintain about 7% of intraseasonal precipitation, with a correlation of 0.79. Araligidad and Maloney (2008) and Dellaripa and Maloney (2015) found similar results with fluxes estimated with mooring data in other tropical regions.

Latent heat flux–precipitation regression slopes for E3SMv1 and CESM2 are shown in Figures 2a,b. E3SMv1 and CESM2 both overestimate the regression slope for their original flux values (11.3%±0.8% and 9.3%±0.6%, respectively). With COARE-estimated fluxes, E3SMv1 and CESM2 regression slopes are reduced to 9.7%±0.7% and 8.2%± 0.6%, respectively, in closer agreement to observations. The change is statistically significant with 99% confidence for E3SMv1, and 95% confidence for CESMs. The smaller regression coefficient with the offline-corrected fluxes suggests that surface fluxes simulated with the original bulk flux schemes in E3SMv1 and CESM2 may artificially maintain intraseasonal convection in those models.

To explore how surface flux changes might affect intraseasonal precipitation elsewhere in the Warm Pool, we calculated regression coefficients for the original and corrected flux time series at each grid point for each model. The spatial patterns and magnitudes of regression slope are similar between the two models (Figure 2c, d), with positive values located mainly south of the equator, consistent with the typical MJO propagation pathway for this time of year (Kim et al., 2017). Changes to the regression slope when using the offline-corrected fluxes are shown in Figure 2e, f). For E3SMv1, the offline correction yields both positive and negative changes to the regression slope, while the changes are mostly negative for CESM2.

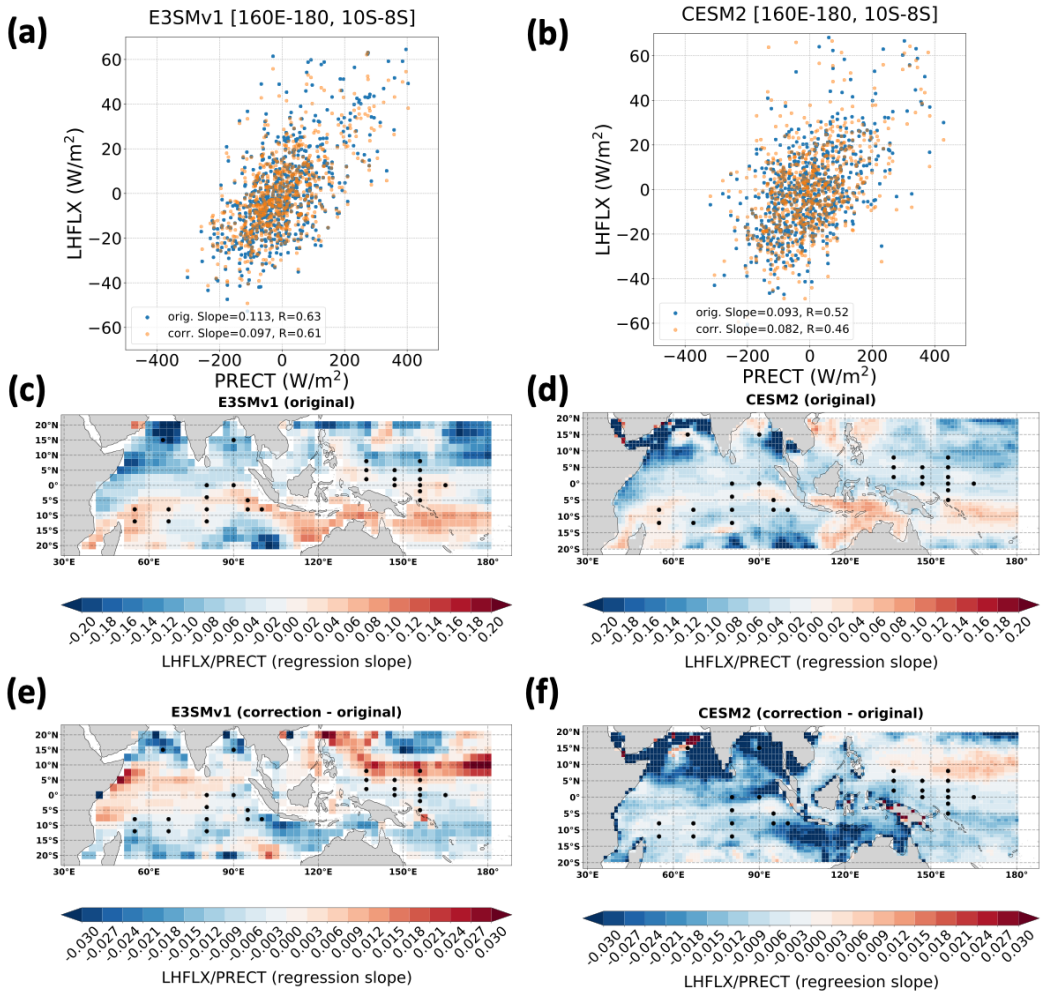

Figure 2. The scatter plot of November–April precipitation and latent heat flux anomalies (units of W m^{-2} for both) averaged over 160°E-180° and 10°S-8°S for (a) E3SMv1 and (b) CESM2. Blue and orange dots correspond to original and offline-corrected latent heat fluxes, respectively. The linear regression for both are shown in the legend. (c, d) maps of the regression coefficient (unitless) at each grid point for the original surface flux and (e, f) maps of regression slope changes after applying the flux correction. Black dots show locations of TAO/TRITON and RAMA moorings used to construct the flux matrix shown in Figure 1a.

There are at least two possible reasons for the more widespread increase of the regression slope in E3SMv1 as compared to CESM2. Foremost, since the latent heat correction performed in our analysis is determined by the binned $|\mathbf{V}|$ and Δq, the spatially varying slope differences between the two models must relate to differences in the spatial and temporal distributions of these variables between the two models. Some of the difference, however, may arise from small differences in the true values of $|\mathbf{V}|$ and Δq in E3SMv1 and our estimations of those quantities from their 1000 hPa surrogates (see Supplement). However, we emphasize that the differences in regression slope changes with flux correction are generally smaller than 3%, while the baseline regression slopes are mostly in the range of 9–12%.

For both models, positive changes in regression slope are mainly located in areas with negative regression slopes in Figure 2c and d), and vice versa. This shows that the models tend to overestimate the magnitude of the regression slopes no matter if they are positive or negative. Furthermore, for both models, flux correction leads to larger decreases in regression slopes in the subtropics (i.e., poleward of about 10° latitude) than in the deep tropics (10°S–10°N) across the Indian Ocean and extending as far east as 120°E. This suggests that corrected surface fluxes for these longitudes would be less supportive of intraseasonal rainfall in the subtropics than in the deep tropics.

Finally, we examine how flux correction might change surface fluxes within the MJO lifecycle by regressing lagged flux and precipitation anomaly time series averaged from 15°S–15°N onto 20–100 day filtered precipitation at a base point in the eastern Indian Ocean (85°E-95°E and 5°S-5°N). For the coupled simulations shown in Figure 3, MJO precipitation in both models exhibits eastward propagation typical of many climate models (Ahn et al., 2020). Latent heat flux anomalies (shading in Figure 3) in E3SMv1 are positive over much of the Indian Ocean from lag 0 to lag 10. In contrast, fluxes in CESM2 are mostly negative, except for smaller positive patches near the MJO convection center at lag 0, and gradually expanding westward by lag 10. Replacing each model's original flux with the COARE-estimated flux yields non-uniform changes to the fluxes across the MJO lifecycle (Figure 3c, d), reducing the flux during enhanced rainfall, and increasing the flux during suppressed rainfall. In both simulations, the COARE-estimated flux contributes less column moistening during the MJO active phase (positive rainfall anomalies) and more column moistening during its suppressed phase (negative rainfall anomalies). This suggests that, compared to the models' original fluxes, COARE-estimated fluxes would be slightly more supportive of MJO eastward propagation and less supportive of MJO maintenance.

5 Inline correction of latent heat flux and effect on simulated MJO

Here, we examine the effects of the COARE algorithm on intraseasonal precipitation using an inline correction. Two atmosphere-only simulations of both models were performed, one with the original flux algorithm, and one with the COARE3.0 algorithm. Reeves Eyre et al. (2021) provided output from the E3SM atmosphere-only simulations. In these six-year simulations, the model was forced with a repeating cycle of observed monthly SSTs from the year 2000. We then performed a pair of 20-year simulations with the atmospheric component of CEMS2 with the original and the COARE3.0 algorithm using the same code modifications as in Reeves Eyre et al. (2021) and forced with observed SSTs from 1979-2009. We refer to these simulations as E3SM_climo and CESM2_amip to distinguish them from the coupled simulations analyzed with our offline corrections (Section 4).

We find statistically significant changes with 90% confidence in the flux-precipitation regression slope in E3SM_climo (12.8%±0.7% and 11.6%±0.8%, respectively) but not in CESM2_amip (12.3% ± 0.3% and 11.9% ± 0.4%, respectively) in the regional averaged analysis (160°E-180° and 10°S-8°S; Supplementary Figure 1a, b). Overestimation

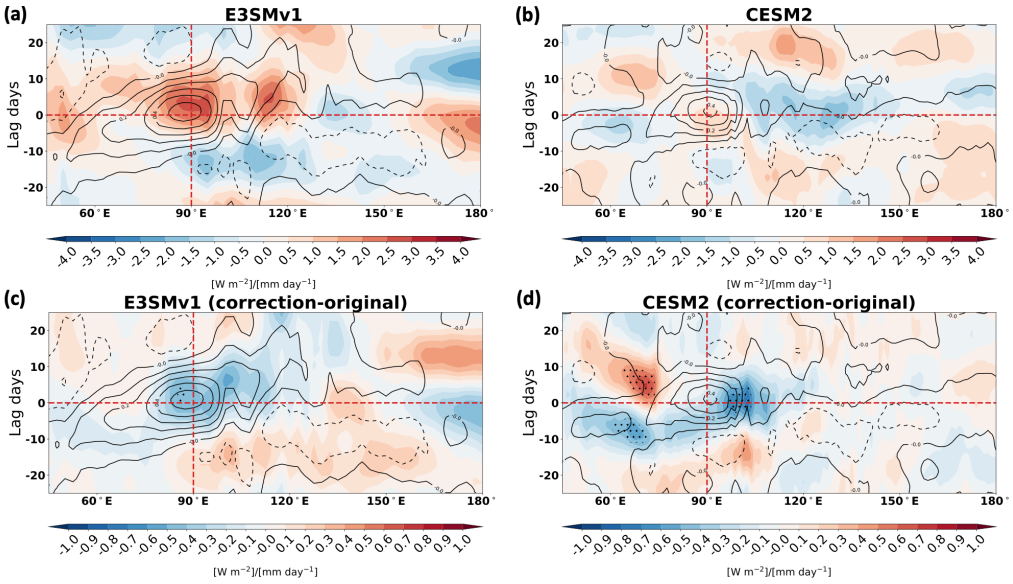

Figure 3. The lead-lag Hovmoller diagram of precipitation (contour with 0.1 interval) and latent heat flux (shaded) regression with base point mean precipitation (5°S-5°N and 85°E-95°E) during November to April in (a) E3SMv1 with original bulk flux algorithm, (b) CESM2 with original bulk flux algorithm, and offline corrected latent heat fluxes minuses original latent heat fluxes in (c) E3SMv1 and (d) CESM2 with stippled regions showing the differences are significant with 90 % confidence interval.

of the regression slope in both models is magnified compared to the coupled simulations (Figure 2a, b), likely due to the missing feedback of SST cooling in the coupled simulations. However, both simulations show decreased regression slopes after changing to the COARE algorithm. This effect is consistent over much of the tropics (Supplementary Figure 1c–f), but less so for E3SM_climo, where COARE fluxes are more supportive of MJO convection across the equatorial Indian Ocean. With COARE, regression slopes become slightly more positive over the Maritime Continent for both models.

We next examine the effect of the COARE algorithm on the evolution of intraseasonal precipitation and surface fluxes. In contrast to the eastward propagating signal seen in the coupled simulations (Figure 3), precipitation in the atmosphere-only simulations exhibits distinct westward propagation for both E3SM_climo simulations (Figure 4a, c) and for the CESM2_amip simulation with the original flux algorithm Figure 4b). This is consistent with the well-known tendency for uncoupled simulations to struggle with simulating eastward propagating intraseasonal signals compared to coupled simulations of the same model ((DeMott et al., 2015) and references therein). For E3SM_climo, the effect is likely further exaggerated by a lack of interannual SST variability that has been shown to bolster MJO eastward propagation in climate models (Klingaman & DeMott, 2020). Compared to the simulation with the original flux algorithm, the CESM2_amip simulation with COARE fluxes (Figure 4d) produces noticeably less westward propagation, yielding a mostly standing oscillation.

Changes to surface fluxes across the intraseasonl precipitation oscillation are most apparent when comparing flux changes east and west of 90°E at lag 0. At this lag, precipitation is more suppressed to the east, and more enhanced to the west (Figures 4a–d). Changing to the COARE flux algorithm leads to enhanced surface fluxes near and east of precipitation and reduced fluxes west of precipitation. These changes are qual-

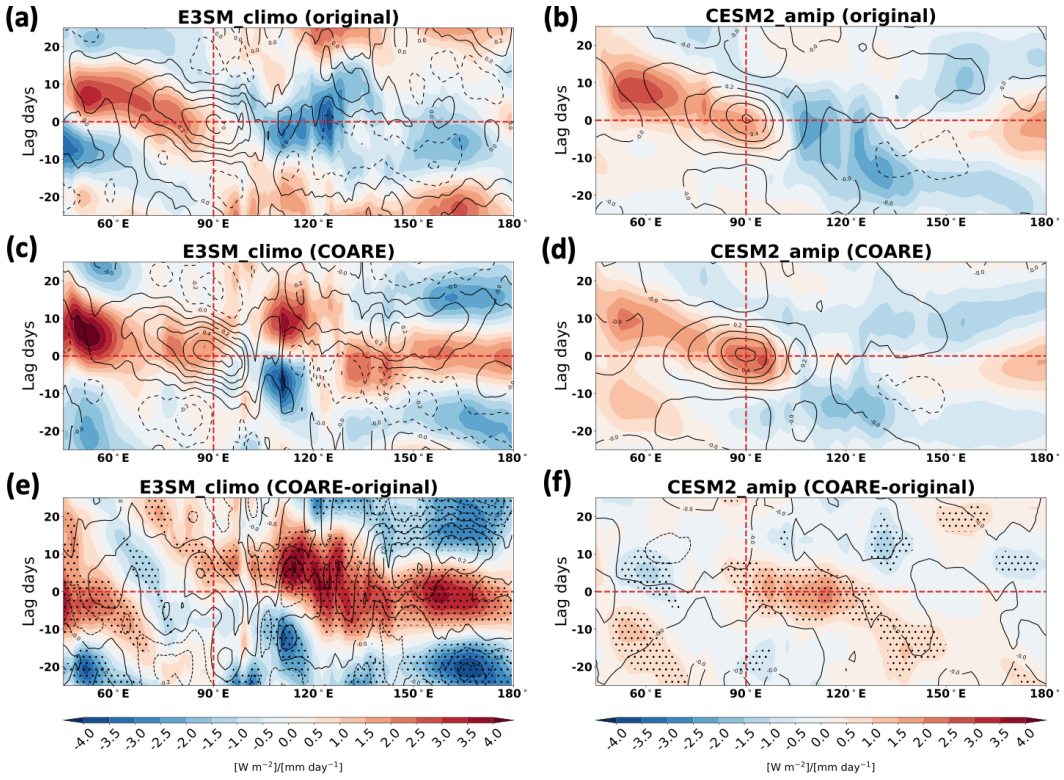

Figure 4. The lead-lag Hovmoller diagram of precipitation (contour with 0.1 interval) and latent heat flux (shaded) regression with base point mean precipitation (5°S-5°N and 85°E-95°E) during November to April in (a) E3SM_climo with original bulk flux algorithm, (b) CESM2_amip with original bulk flux algorithm, (c) E3SM_climo with COARE bulk flux algorithm, (d) CESM2_amip with COARE bulk flux algorithm, (e) (c) minuses (a), and (f) (d) minuses (b) with stippled regions showing the differences are significant with 95 % confidence interval.

itatively similar to those for the offline flux correction (Figure 3c, d) and offer further support for the idea that COARE fluxes may encourage MJO eastward propagation by enhancing column moistening to the east of precipitation and reducing it to the west.

6 Summary and Conclusions

In this study, we develop a simple diagnostic method to illustrate surface fluxes based on bulk algorithm inputs ($|\mathbf{V}|$ and Δq) and then use this diagnostic to compute surface flux biases. Compared to western tropical Pacific surface fluxes computed with in situ observations and the COARE3.0 bulk flux algorithm, which well-estimates directly measured surface fluxes (Brunke et al., 2003), surface fluxes in the E3SMv1 and CESM2 climate models are too large at very low and very high wind speeds.

To investigate how this difference in latent heat flux might affect the MJO, we used our flux matrix diagnostic to adjust model-simulated fluxes to COARE-estimated fluxes within each $|\mathbf{V}|$–Δq bin (i.e., the offline correction). We found that this adjustement reduced the latent heat flux support of intraseaonal precipitation in both models, bringing it closer to observations. Longitude-lagged precipitation and latent heat flux composites reveal that offline flux correction increases the flux during the MJO convectively

suppressed phase and reduces the flux during the MJO convectively active phase, suggesting that fluxes computed with the COARE algorithm are less supportive of MJO convection and may help promote MJO eastward propagation.

To test this idea, we analyzed the latent heat flux–precipitation relation in atmosphere-only simulations with E3SM_climo and CESM2_amip with the original and the COARE bulk flux algorithms (i.e., the inline correction). Similar to the results with the offline corrections, surface fluxes with the COARE algorithm were also less supportive of intraseasonal convection, in better agreement with observations. The effect of COARE surface fluxes on the MJO propagation was difficult to assess, since both models simulate strong westward propagating disturbances in these uncoupled simulations. However, COARE fluxes in CESM2_amip did reduce westward propagation in that model.

Our findings suggest that MJO simulation in climate models may be sensitive to the choice of algorithm for computing surface fluxes. This has several implications. First, as the MJO regulates extreme weather over much of the globe via teleconnections (Stan et al., 2017), changes to MJO amplitude and propagation will affect these teleconnections. Second, if COARE surface fluxes contribute to enhanced MJO eastward propagation in fully coupled simulations, as our results here suggest they should, this could increase the number of simulated MJO events that reach the western Pacific Ocean, where its low-level westerly wind anomalies can initiate oceanic Kelvin waves that help expand the eastern edge of the Warm Pool (Puy et al., 2016) and contribute to the onset of El Niño events (Hendon et al., 2007). Finally, updating the bulk surface flux algorithm in coupled models will affect ocean-atmosphere coupled processes globally. Indeed, Reeves Eyre et al. (2021) found statistically significant changes to mean cloud fields and cloud radiative effects with the COARE algorithm in the E3SM_climo experiments analyzed in our study. To explore how changes in the bulk flux algorithm are manifested in fully coupled simulations, we are running coupled simulations of the E3SM with the COARE bulk flux algorithm.

Acknowledgments

Hsu and DeMott were supported by DOE RGMA grant DE-SC0020092. DeMott also received support from NOAA MAPP NA20OAR4310389. This research used resources of the National Energy Research Scientific Computing Center (NERSC), a U.S. Department of Energy Office of Science User Facility located at Lawrence Berkeley National Laboratory, operated under Contract No. DE-AC02-05CH11231 and high-performance computing support from Cheyenne (doi:10.5065/D6RX99HX) provided by NCAR's Computational and Information Systems Laboratory, sponsored by the National Science Foundation.

TAO mooring data were provided by the Global Tropical Moored Buoy Array (`https://www.pmel.noaa.gov/tao/drupal/disdel/`). E3SM Project, DOE. Energy Exascale Earth System Model v1.0. Computer Software is available at `https://github.com/E3SM-Project/E3SM/releases/tag/v1.0.0` since 23 Apr. 2018 with Web doi:10.11578/E3SM/dc.20180418.36. and the raw model output is available at `https://portal.nersc.gov/archive/home/j/jeyre/www/`. Instruction for downloading CESM2 model code can be found at `https://www.cesm.ucar.edu/models/cesm2/release_download.html` and the raw model output can be found at Earth System Grid Federation at `https://esgf-node.llnl.gov/projects/cmip6/`. Data used to create the figures in this article are available at `http://dx.doi.org/10.25675/10217/234033`.

References

Ahn, M.-S., Kim, D., Kang, D., Lee, J., Sperber, K. R., Gleckler, P. J., ... Kim, H. (2020). MJO Propagation Across the Maritime Continent: Are CMIP6

Models Better Than CMIP5 Models? *Geophysical Research Letters*, *47*(11), e2020GL087250. doi: 10.1029/2020GL087250

Araligidad, N. M., & Maloney, E. D. (2008). Wind-driven latent heat flux and the intraseasonal oscillation. *Geophysical Research Letters*, *35*(4). doi: 10.1029/2007GL032746

Bourassa, M. A., Vincent, D. G., & Wood, W. L. (1999, May). A Flux Parameterization Including the Effects of Capillary Waves and Sea State. *Journal of the Atmospheric Sciences*, *56*(9), 1123–1139. doi: 10.1175/1520-0469(1999)056⟨1123:AFPITE⟩2.0.CO;2

Brodeau, L., Barnier, B., Gulev, S. K., & Woods, C. (2017, January). Climatologically Significant Effects of Some Approximations in the Bulk Parameterizations of Turbulent Air–Sea Fluxes. *Journal of Physical Oceanography*, *47*(1), 5–28. doi: 10.1175/JPO-D-16-0169.1

Brunke, M. A., Fairall, C. W., Zeng, X., Eymard, L., & Curry, J. A. (2003, February). Which Bulk Aerodynamic Algorithms are Least Problematic in Computing Ocean Surface Turbulent Fluxes? *Journal of Climate*, *16*(4), 619–635. doi: 10.1175/1520-0442(2003)016⟨0619:WBAAAL⟩2.0.CO;2

Bui, H. X., Maloney, E. D., Dellaripa, E. M. R., & Singh, B. (2020). Wind Speed, Surface Flux, and Intraseasonal Convection Coupling From CYGNSS Data. *Geophysical Research Letters*, *47*(21), e2020GL090376. doi: 10.1029/2020GL090376

Danabasoglu, G., Lamarque, J.-F., Bacmeister, J., Bailey, D. A., DuVivier, A. K., Edwards, J., ... Strand, W. G. (2020). The Community Earth System Model Version 2 (CESM2). *Journal of Advances in Modeling Earth Systems*, *12*(2), e2019MS001916. doi: 10.1029/2019MS001916

Dellaripa, E. M. R., & Maloney, E. D. (2015). Analysis of MJO Wind-Flux Feedbacks in the Indian Ocean Using RAMA Buoy Observations. *Journal of the Meteorological Society of Japan. Ser. II*, *93A*, 1–20. doi: 10.2151/jmsj.2015-021

DeMott, C. A., Benedict, J. J., Klingaman, N. P., Woolnough, S. J., & Randall, D. A. (2016). Diagnosing ocean feedbacks to the MJO: SST-modulated surface fluxes and the moist static energy budget. *Journal of Geophysical Research: Atmospheres*, *121*(14), 8350–8373. doi: 10.1002/2016JD025098

DeMott, C. A., Klingaman, N. P., & Woolnough, S. J. (2015). Atmosphere-ocean coupled processes in the Madden-Julian oscillation. *Reviews of Geophysics*, *53*(4), 1099–1154. doi: 10.1002/2014RG000478

de Szoeke, S. P., Edson, J. B., Marion, J. R., Fairall, C. W., & Bariteau, L. (2015, January). The MJO and Air–Sea Interaction in TOGA COARE and DYNAMO. *Journal of Climate*, *28*(2), 597–622. doi: 10.1175/JCLI-D-14-00477.1

de Szoeke, S. P., Yuter, S., Mechem, D., Fairall, C. W., Burleyson, C. D., & Zuidema, P. (2012, December). Observations of Stratocumulus Clouds and Their Effect on the Eastern Pacific Surface Heat Budget along 20°S. *Journal of Climate*, *25*(24), 8542–8567. doi: 10.1175/JCLI-D-11-00618.1

Donlon, C. J., & the GHRSST-PP Science Team. (2005). *The Recommended GHRSST-PP Data Processing Specification GDS (version 1 revision 1.6).* The GHRSST-PP International Project Office, Exeter, U.K.

Edson, J. B., Jampana, V., Weller, R. A., Bigorre, S. P., Plueddemann, A. J., Fairall, C. W., ... Hersbach, H. (2013, August). On the Exchange of Momentum over the Open Ocean. *Journal of Physical Oceanography*, *43*(8), 1589–1610. doi: 10.1175/JPO-D-12-0173.1

Eyring, V., Bony, S., Meehl, G. A., Senior, C. A., Stevens, B., Stouffer, R. J., & Taylor, K. E. (2016, May). Overview of the Coupled Model Intercomparison Project Phase 6 (CMIP6) experimental design and organization. *Geoscientific Model Development*, *9*(5), 1937–1958. doi: 10.5194/gmd-9-1937-2016

Fairall, C. W., Bradley, E. F., Hare, J. E., Grachev, A. A., & Edson, J. B. (2003,

February). Bulk Parameterization of Air–Sea Fluxes: Updates and Verification for the COARE Algorithm. *Journal of Climate*, *16*(4), 571–591. doi: 10.1175/1520-0442(2003)016⟨0571:BPOASF⟩2.0.CO;2

Golaz, J.-C., Caldwell, P. M., Roekel, L. P. V., Petersen, M. R., Tang, Q., Wolfe, J. D., ... Zhu, Q. (2019). The DOE E3SM Coupled Model Version 1: Overview and Evaluation at Standard Resolution. *Journal of Advances in Modeling Earth Systems*, *11*(7), 2089–2129. doi: 10.1029/2018MS001603

Hendon, H. H., Wheeler, M. C., & Zhang, C. (2007, February). Seasonal Dependence of the MJO–ENSO Relationship. *Journal of Climate*, *20*(3), 531–543. doi: 10.1175/JCLI4003.1

Kiladis, G. N., Wheeler, M. C., Haertel, P. T., Straub, K. H., & Roundy, P. E. (2009). Convectively coupled equatorial waves. *Reviews of Geophysics*, *47*(2). doi: 10.1029/2008RG000266

Kim, D., Kim, H., & Lee, M.-I. (2017). Why does the MJO detour the Maritime Continent during austral summer? *Geophysical Research Letters*, *44*(5), 2579–2587. doi: 10.1002/2017GL072643

Klingaman, N. P., & DeMott, C. A. (2020). Mean State Biases and Interannual Variability Affect Perceived Sensitivities of the Madden-Julian Oscillation to Air-Sea Coupling. *Journal of Advances in Modeling Earth Systems*, *12*(2), e2019MS001799. doi: 10.1029/2019MS001799

Large, W. G., & Yeager, S. G. (2004). *Diurnal to Decadal Global Forcing for Ocean and Sea-Ice Models: The Data Sets and Flux Climatologies.* NCAR Tech. Note NCAR/TN-460+STR, University Corporation for Atmospheric Research.

Large, W. G., & Yeager, S. G. (2009, August). The global climatology of an interannually varying air–sea flux data set. *Clim Dyn*, *33*(2), 341–364. doi: 10.1007/s00382-008-0441-3

Madden, R. A., & Julian, P. R. (1971, July). Detection of a 40–50 Day Oscillation in the Zonal Wind in the Tropical Pacific. *Journal of the Atmospheric Sciences*, *28*(5), 702–708. doi: 10.1175/1520-0469(1971)028⟨0702:DOADOI⟩2.0.CO;2

Madden, R. A., & Julian, P. R. (1972, September). Description of Global-Scale Circulation Cells in the Tropics with a 40–50 Day Period. *Journal of the Atmospheric Sciences*, *29*(6), 1109–1123. doi: 10.1175/1520-0469(1972)029⟨1109:DOGSCC⟩2.0.CO;2

Matsugishi, S., Miura, H., Nasuno, T., & Satoh, M. (2020). Impact of latent heat flux modifications on the reproduction of a Madden–Julian oscillation event during the 2015 Pre-YMC campaign using a global cloud-system-resolving model. *Sola*, *advpub*. doi: 10.2151/sola.16A-003

McPhaden, M., Ando, K., Bourles, B., Freitag, H., Lumpkin, R., Masumoto, Y., ... Yu, W. (2010, December). The Global Tropical Moored Buoy Array. In *Proceedings of OceanObs'09: Sustained Ocean Observations and Information for Society* (pp. 668–682). European Space Agency. doi: 10.5270/OceanObs09.cwp.61

McPhaden, M., Busalacchi, A., Cheney, R., Donguy, J., Gage, K., Halpern, D., ... Takeuchi, K. (1998). The Tropical Ocean-Global Atmosphere observing system: A decade of progress. doi: 10.1029/97JC02906

Puy, M., Vialard, J., Lengaigne, M., & Guilyardi, E. (2016, April). Modulation of equatorial Pacific westerly/easterly wind events by the Madden–Julian oscillation and convectively-coupled Rossby waves. *Clim Dyn*, *46*(7), 2155–2178. doi: 10.1007/s00382-015-2695-x

Redelsperger, J.-L., Guichard, F., & Mondon, S. (2000, January). A Parameterization of Mesoscale Enhancement of Surface Fluxes for Large-Scale Models. *Journal of Climate*, *13*(2), 402–421. doi: 10.1175/1520-0442(2000)013⟨0402:APOMEO⟩2.0.CO;2

Reeves Eyre, J. E. J., Zeng, X., & Zhang, K. (2021). Ocean Surface Flux Algorithm Effects on Earth System Model Energy and Water Cycles. *Front. Mar. Sci.*, *8*. doi: 10.3389/fmars.2021.642804

Stan, C., Straus, D. M., Frederiksen, J. S., Lin, H., Maloney, E. D., & Schumacher, C. (2017). Review of Tropical-Extratropical Teleconnections on Intraseasonal Time Scales. *Reviews of Geophysics*, *55*(4), 902–937. doi: 10.1002/2016RG000538

Yadav, P., & Straus, D. M. (2017, May). Circulation Response to Fast and Slow MJO Episodes. *Monthly Weather Review*, *145*(5), 1577–1596. doi: 10.1175/MWR-D-16-0352.1

Yasunaga, K., Yokoi, S., Inoue, K., & Mapes, B. E. (2019, January). Space–Time Spectral Analysis of the Moist Static Energy Budget Equation. *Journal of Climate*, *32*(2), 501–529. doi: 10.1175/JCLI-D-18-0334.1

Zeng, X., Zhao, M., & Dickinson, R. E. (1998, October). Intercomparison of Bulk Aerodynamic Algorithms for the Computation of Sea Surface Fluxes Using TOGA COARE and TAO Data. *Journal of Climate*, *11*(10), 2628–2644. doi: 10.1175/1520-0442(1998)011⟨2628:IOBAAF⟩2.0.CO;2

Zhang, C., & Dong, M. (2004, August). Seasonality in the Madden–Julian Oscillation. *Journal of Climate*, *17*(16), 3169–3180. doi: 10.1175/1520-0442(2004)017⟨3169:SITMO⟩2.0.CO;2

Supporting Information for Ocean Surface Flux Algorithm Effects on Tropical Indo-Pacific Intraseasonal Precipitation

Chia-Wei Hsu [1], Charlotte A. DeMott, Mark D. Branson[1], Jack Reeves Eyre[2], and Xubin Zeng[3]

[1]Colorado State University

[2]Cooperative Institute for Climate, Ocean and Ecosystem Studies, University of Washington

[3]University of Arizona

Contents of this file

1. Text S1
2. Figures S1

Introduction The supplementary information includes the text explaining the derivation of the surface variables based on the 1000 hPa field in E3SMv1 coupled simulation and the figure showing the relationship between latent heat flux and intra-seasonal precipitation in the E3SM_climo and CESM2_amip simulations.

Text S1 Surface variables for E3SMv1 CMIP6 simulation: The simulation provides $|\mathbf{V}|$ and q at 1000 hPa. Following de Szoeke et al., (2012), we use the Monin-Obukhov Similarity Theory to estimate T_{sfc} and q_{2m} for the simulation. Following their approach,

we use the wind velocity and specific humidity at 1000hPa to derive the surface values based on

$$u_{10m} = \frac{u^*}{k}(\ln(\frac{10}{z_0}) - \Psi(\frac{10}{L})) \tag{1}$$

$$q_{2m} = q(1000\text{hPa}) + \frac{q^*}{k}(\ln(\frac{z(1000\text{hPa})}{2}) + \Psi(\frac{2}{L}) - \Psi(\frac{z(1000\text{hPa})}{L})) \tag{2}$$

, where k is the von Kármán constant, L the Monin–Obukhov length, stability parameters q^* and u^* which parameterized the vertical turbulence flux are iteratively derived, and Ψ is determined by the stability condition based on L. We also adjust the background mean field of the derived daily q_{2m} and u_{10m} to their mean values obtained from the monthly output from the E3SMv1 historical simulation in the CMIP6 repository.

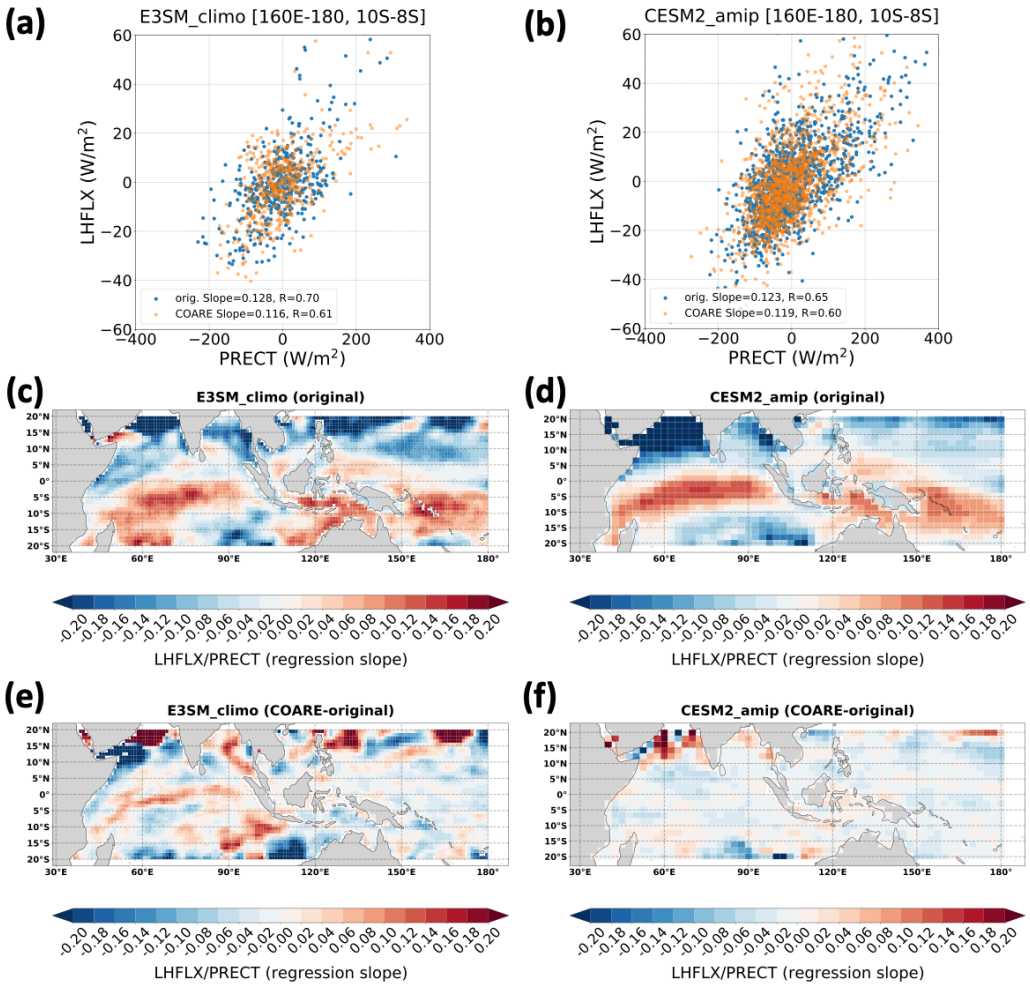

Figure S1. The scatter plot of mean precipitation and mean latent heat flux over the 160°E-180° and 10°S-8°S region in the unit of W/m^2 during Nov-Apr of each year in (a) E3SM_climo and (b) CESM2_amip simulations. The blue dot represents the latent heat flux determined using the original bulk flux algorithm while the orange dot represents the COARE bulk flux algorithm. The linear regression for both original and COARE result are shown in the legend. The map of regression slope value at each grid point during Nov-Apr of each year in (c) E3SM_climo and (d) CESM2_amip simulations based on the original bulk flux algorithm in the models. The map of regression slope changes after the latent heat flux is determined based on the COARE bulk flux algorithm in (e) E3SM_climo and (f) CESM2_amip simulations.